Journal of Solid State Electrochemistry (2024) 28:555–563
https://doi.org/10.1007/s10008-023-05619-2

ORIGINAL PAPER

Hydrogels and their composites based on sulfo-containing acrylates: preparation, properties, and proton conductivity

Rymsha Kh. V.[1,2] · Yevchuk I. Yu.[1] · Zhyhailo M. M.[1] · Demchyna O. I.[1] · Maksymych V. M.[3] · Ivashchyshyn F. O.[3,4]

Received: 28 March 2023 / Revised: 26 July 2023 / Accepted: 26 July 2023 / Published online: 13 October 2023

Abstract

This work presents a method for the synthesis of multifunctional hydrogels based on polymer framework obtained by UV-initiated polymerization of the acrylic monomers (acrylamide, acrylonitrile, and sulfo-group-containing monomer (3-sulfopropyl acrylate potassium salt, 2-acrylamido-2-methylpropane sulfonic acid, and sodium styrene sulfonate)) in the presence of *N*,*N*′-methylenebisacrylamide as a cross-linking agent. Composite polymer/silica nanogels have been created in situ using a TEOS-based sol–gel system and the above-mentioned polymeric matrices. The synthesized material characteristics such as composition, morphology, and thermal stability were explored with FTIR, SEM, and DCS. In addition, the effect of temperature, inorganic component content, sulfo-group-containing monomer to proton conductivity and water uptake have been explored. The obtained hydrogels possess proton conductivity up to 19 mSm/cm with potential implying for application in electrochemical devices and superabsorbent material. This method is user-friendly and cost-efficient, and proceeds in an aqueous environment under atmospheric conditions without the use of heavy metal catalysts.

Keywords Hydrogel · Sulfo-group-containing monomer · Acrylic monomer · Proton conductivity · UV-initiated polymerization

Introduction

Synthetic hydrogels have gained much attention and continue to be the object of intensive research because they have attractive properties and are considered as a convenient class of materials for application in medicine, pharmaceutics, biotechnology, cosmetic industry, etc. [1–3].

Hydrogels on the basis of synthetic polymers are 3D cross-linked polymeric networks that trap large quantities of water in the polymer matrices (up to 99.9%) mainly by surface tension and other weak interactions, at the same time remain insoluble due to chemical or physical cross-links between individual polymeric chains [1]. Porous structure of hydrogel allows water to freely move across the polymer networks. High water uptake makes hydrogels similar to the objects of nature and causes their enormous valuable applications in bio-related fields as carriers for the controlled release of drugs, catalysts, membranes with adjustable permeability, etc. [4–6].

Recently, there is a technological need for hydrogel materials with special characteristics, for example, high conductivity or ionic exchange property. Conductive hydrogels are of a growing interest as they find the application in many electrochemical solid state ionic devices, such as high-energy density batteries, fuel cells, sensors, electrochemical display devices [7–9] and also for the fabrication of flexible electronics owing to their biocompatibility, adjustable mechanical flexibility, good conductivity, and multiple stimuli-responsive properties [10–12]. In [13] they note that combining conductivity with the mechanical and responsive properties hydrogels have promoted the advances in several

✉ Ivashchyshyn F. O.
fedir.ivashchyshyn@pcz.pl

1 Department of Physical Chemistry of Fossil Fuels of the Institute of Physical-Organic Chemistry and Coal Chemistry Named after L. M, Lytvynenko of the National Academy of Sciences of Ukraine, 3a, Naukova Str, Lviv 79060, Ukraine

2 Currently at the Leibniz Institute of Polymer Research Dresden e.V, Hohe Str, D-01069 Dresden, Germany

3 National Lviv Polytechnic University, 12, Bandery Str, Lviv 79013, Ukraine

4 Czestochowa University of Technology, ul. J.H. Dąbrowskiego 69, 42-201 Częstochowa, Poland

emerging areas such as health diagnosing, electronic skins, soft robotics, and energy conversion.

The design of conductive hydrogels is commonly based on the introduction of electron conductors and/or ions into hydrogel matrices. The authors [1] highlight the advantages of ion-conductive hydrogels compared to electron-conductive ones: they possess ion gradients and transparency, which are highly desirable for energy storage and conversion apparatus like actuators and nanogenerators as well as see-through equipment such as displays and touch panels. Besides, some ion-conductive hydrogels possess water retention capability or anti-freezing property, which improves the durability and environment adaptability of flexible electronics.

There are three categories of materials capable to generate free ions in water can: acids (HCl, H_2SO_4, H_3PO_4), metallic salts (NaCl/Na_2SO_4, KCl, LiCl, $LiClO_4$, $FeCl_3$/$FeNO_3$ etc.) and ionic liquids (1-ethyl-3-methylimidazolium chloride). For example, $HClO_4$ was introduced in poly(vinyl alcohol)-based hydrogel membrane resulting in a high-performance electrochemical capacitor [14]; ion-CHs such as PAM hydrogel containing NaCl/LiCl were employed as the electrolytic elastomer in actuator [15]. The example of the use of ionic liquid for providing hydrogels with ion-conductivity may be the research of Liu J. and coworkers [16], designed a PAM hydrogel containing host–guest interactions between 1-benzyl-3-vinylimidazolium and cucurbit [6] uril as a pressure sensor. This hydrogel could withstand an elongation up to 10,000% and support objects with 2000 times weight of itself.

Current advances in hydrogel technology have led to the development of nanocomposite hydrogels. A wide array of nanomaterials (carbon-based, metallic, ceramic) can be incorporated within the hydrogel network to obtain nanocomposite hydrogels with the desired properties [17–19]. The search for new ways of synthesizing hydrogels is caused by the need for their formation in "soft" conditions. Among the various methods of synthesis, the sol–gel method is of special interest, since it allows obtaining inorganic nanoparticles in situ in a polymer solution without the use of high temperatures. The article [20] describes the synthesis of chitosan hydrogel/SiO_2 and chitin hydrogel/SiO_2 hybrid mesoporous materials obtained by the sol–gel method.

Different polymerization techniques used for hydrogel syntheses allow introduction of the active functional groups into a polymeric network, which can provide conductive properties of the material.

Earlier, we studied proton conductive inorganic/organic membranes to find out the effect of the inorganic component on their properties [21]. In this type of membranes synthesized by us, we managed to achieve a high proton conductivity of the order of 7.6–13.5 mSm/cm.

In this paper, we report the development of the new UV-curable conductive polymer hydrogels based on acrylic monomers and various sulfo-group-containing monomers (SM). The presence of sulfo-groups provides ion conductivity of the materials due to ion transport in polymeric matrix. Nanocomposite membranes were synthesized as well by modification of the polymer hydrogels with SiO_2 formed in sol–gel process in situ. The aim of with study is to in investigated of the hydrogel property changes with exchange of the sulphocomponent in the polymer matrix.

Materials and method of experiment

Materials

Acrylonitrile (AN), acrylamide (AAm), 2-acrylamido-2-methylpropane sulfonic acid (AMPS), 3-sulfopropylacrylate potassium salt (SPAK), sodium 4-vinylbenzenesulfonate (sodium styrene sulfonate) (NaSS), *N,N′*-methylenebisacrylamide (MBA), tetraethoxysilane (TEOS, 99%), and 2,2-dimethoxy-2-phenylacetophenone (DMPA) were purchased from Sigma-Aldrich and used as received (unless otherwise noted). Phosphoric acid (85%, Sigma-Aldrich) (PhA) was used as a catalyst in sol–gel reaction. Milli-Q® water, absolute ethanol (VWR), and acetone (Analytical Grade, Fisher Scientific) were used as solvents.

Synthesis of hydrogels

Polymer hydrogel were synthesized by UV-initiated copolymerization of the mixture of monomers. A typical procedure according to [21] was as follows: a solution of water-soluble reagents was prepared by dissolving them in DW and then mixed with the appropriate amount of AN and DMPA under constant stirring (500 rpm) to form a homogeneous solution. Monomers that contained inhibitor upon purchase were purified through a basic alumina column to remove inhibitor prior to use. The purification of a solid monomer (AAm) containing inhibitor was forgone to conserve material and not dilute polymerization solution beyond optimized concentrations in an effort to run through the alumina plug. The resulting mixture was placed in a handmade glass mold. Polymerization was carried out under UV-irradiation (365 nm, 15 $J \cdot cm^{-2}$) using a multi-lamp BIO-LINK® cross-linker (BLX-365, Witec AG, Switzerland) equipped with five UV lamps (8 W, output 0.8 W). To prevent the inhibiting effect of oxygen on polymerization process, the molds were covered with glass slides. After UV exposure, the obtained membranes were rinsed with acetone and then dried to the constant weight at the oven with temperature 50 °C. The optimal polymerization compositions for the monomers were achieved at SM:AAm:AN:MBA ratio of 9.5:65:25:0.5 mol%.

In case of composite hydrogels, the ratio between monomer mixture and sol–gel system in the compositions for the synthesis of organic/inorganic nanocomposites was 90 wt.% monomer mixture to 10 wt% sol–gel solution. The sol–gel

precursor solution was prepared by mixing of TEOS, ethanol, deionized water (DW), and phosphoric acid with a molar ratio of [TEOS]:[Eth]:[DW]:[PhA] = 1:4:2:1.8. The system was stirred continuously at 500 rpm in 50 °C water bath for 25 min. Then, a sol–gel precursor solution was added to the monomer mixture and stirring (500 rpm) to form a homogeneous solution.

Characterization

To confirm the structure of the synthesized copolymers, a calculation was carried out based on the kinetic data using the Alfrey-Price equation. This method can be used to describe the process of copolymer formation with sufficient reliability. Since the monomers which take place in the copolymerization process have different activities and are involved in the copolymers in different quantities depending on the degree of conversion, we can conclude that the synthesized copolymers have statistical structure.

The FTIR/ATR spectra were examined in 4000–600 cm^{-1} range by FTIR Microscope Hyperion 2000 (Bruker, Germany) equipped with both MCT detector and ATR objective coupled to FTIR spectrometer Vertex 70 (Bruker, Germany). The baselines were corrected and the spectra were normalized with respect to the band of stretching vibration of nitrile group (2243 cm^{-1}).

SEM images of the membranes were obtained using NEON 40 FIB-SEM scanning electron microscope (Carl Zeiss Microscopy GmbH, Germany). Before imaging, all the membranes were coated with ≈ 20 nm thick Pt layer to reduce charging in the electron beam. For cross-sectional imaging, the membranes were fractured in liquid nitrogen.

TGA of the samples was performed using Q5000 thermal analyzer (TA Instruments, USA) in the temperature range 30 – 800 °C at heating rate of 10 °C min^{-1}.

DSC measurements were carried out using DSC 2500 thermal analyzer (TA Instruments, USA). The DSC scans were run under a dynamic nitrogen atmosphere from – 80 to 150 °C at heating and cooling rates of 10 °C min^{-1}. Glass transition temperature (T_g) values were determined from the second cooling run.

WU was determined gravimetrically. The samples of the prepared membranes were dried at 20 °C under vacuum until constant weight, weighed, and placed into deionized water for 24 h. Then, the samples were taken out from water, and finally, wiped with filter paper and weighed. WU was calculated as the difference between the weights of the dry and wet samples.

Proton conductivity (PC) of the membranes was measured using the impedance spectroscope Autolab/FRA-2 (the Netherlands) in the frequency range of 10 – 10^5 Hz. The tested sample was sandwiched between two Pt electrodes. The values of the specific proton conductance were calculated using equation:

$$\sigma = l/RS(\mathrm{Sm/cm}) \quad (1)$$

where R is the sample resistance, Ohm; S is the electrode—sample contact area, cm^2. l is the thickness of the specimen, cm.

Results and discussion

It is known that ionic groups –SO_3H are the best for ensuring a high level of conductivity, so it was interesting to explore polymer and composite hydrogels based on different sulfo-containing monomers and compare their properties. There are reports on the preparation of conductive polyelectrolytes with high level of conductivity based on 2-acrylamido-2-methylpropane sulfonic acid and 4-vinylbenzenesulfonate (sodium styrene sulfonate) [22, 23]. We tried to use 3-sulfopropylacrylate potassium salt for this purpose as well. Despite of the previous our study, there are only a few publications on the synthesis of conductive materials based on this sulfo-group-containing monomers [24, 25].

Due to the presence of acrylic fragments in the molecules of the chosen monomers, UV-initiated polymerization of these monomers could have been easily conducted. The statistical copolymer with a cross-linked structure was produced as the result of polymerization process (see Fig. 1). The polymer hydrogels using various sulfo-containing monomers were prepared: AMPS-PH, NaSS-PH, and SPAK-PH. The composite hydrogels were obtained with addition of the appropriate amounts of sol–gel system to the polymerization compositions before gelation [25], since formation of inorganic nanoparticles in polymer matrices took place in situ simultaneously with the polymerization process.

Generally, the FTIR spectra (Fig. 2) for the polymer series of the hydrogel with varied SM have the same pattern and are similar to each other. The results can be explained by the fact that polymer matrices in major are the same. Furthermore, the presence of the differentiable functional groups causes the appearance additional peaks.

Two absorption peaks are observed at around 3341 cm^{-1} and 3196 cm^{-1}, which belong to the symmetric and asymmetric stretching vibrations of ν(N–H) of free and bound primary amines, respectively. In the case of AMPS containing hydrogel, the peak at 3341 cm^{-1} is more intense due to the presence of a secondary amine group [26, 27] . In addition, the partially overlapped peaks at 3428 cm^{-1} may be attributed to O–H stretching vibrations of water and reflect the hydrophilicity of the materials. The stretching asymmetric and symmetric vibrations $\nu(C-H)$ in CH, CH_2, and CH_3 groups of hydrocarbon chain are registered in the range of 2940–2790 cm^{-1}. The analysis of the obtained spectra shows the peak at 2243 cm^{-1} corresponds to stretching vibration of CN group and indicates

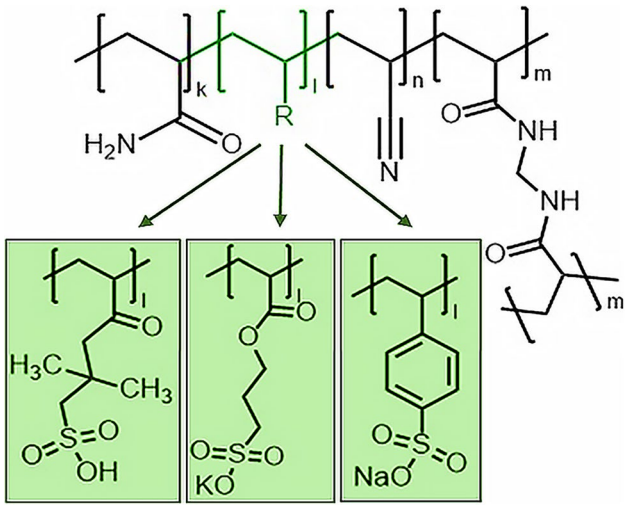

Fig. 1 Scheme of polymer hydrogel structure with various sulfo-group-containing monomer units

the presence AN in thy hydrogels structure. FTIR spectra also show the peaks at 1657 cm^{-1} and "shoulders" at 1614 cm^{-1}, which correspond to vibrations of amide I groups, and the peaks at 1554 cm^{-1}—vibrations of amide II groups, which are characteristics of primary amides. The vibration band of amide II is partially masked by the intense absorption band of carbonyl group of amide II.

In contrast to the other two, in the spectrum from SPAK, there is the peak at 1720 cm^{-1} associated with the C–O–C bond. Only in the case of FTIR spectrum of SSNa containing hydrogel, the peak at 1557 cm^{-1} is observed, which is inherent to the stretching vibrations of the bonds in the aromatic ring, and at 623 cm^{-1} is the absorption band of non-planar C–H deformation vibrations of benzene ring. It should be noted that the absorption bands with the peaks at 1180, 1125, and 1040 cm^{-1} refer to the stretching vibrations of sulfo-groups $\nu(S=O)$, indicating the copolymerization of each of the sulfo-group-containing monomers into the polymer framework. Since the absorption bands of the asymmetric stretching vibration of Si–O–Si groups at 1206 cm^{-1} are masked, the broad absorption band with the peak at 995 cm^{-1} (in the case of SPAK-PH-SG10 membrane there is a noticeable shift to 985 cm^{-1}), attributed for the stretching vibrations of Si–OH, allows us to conclude about the successful introduction of an inorganic component.

As can be seen from the SEM images (Fig. 3), polymer hydrogel morphologies suffer from significant and complicated changes after replacement of sulfo-component. The polymer hydrogel with SPAK content has the uniform structure and the fragile fracture, compare with the asymmetric laminar two- and three-layer structure observed in the NaSS and AMPS containing hydrogels.

The three layers of the laminar structure of AMPS-PH can be noticed by the difference in the texture and

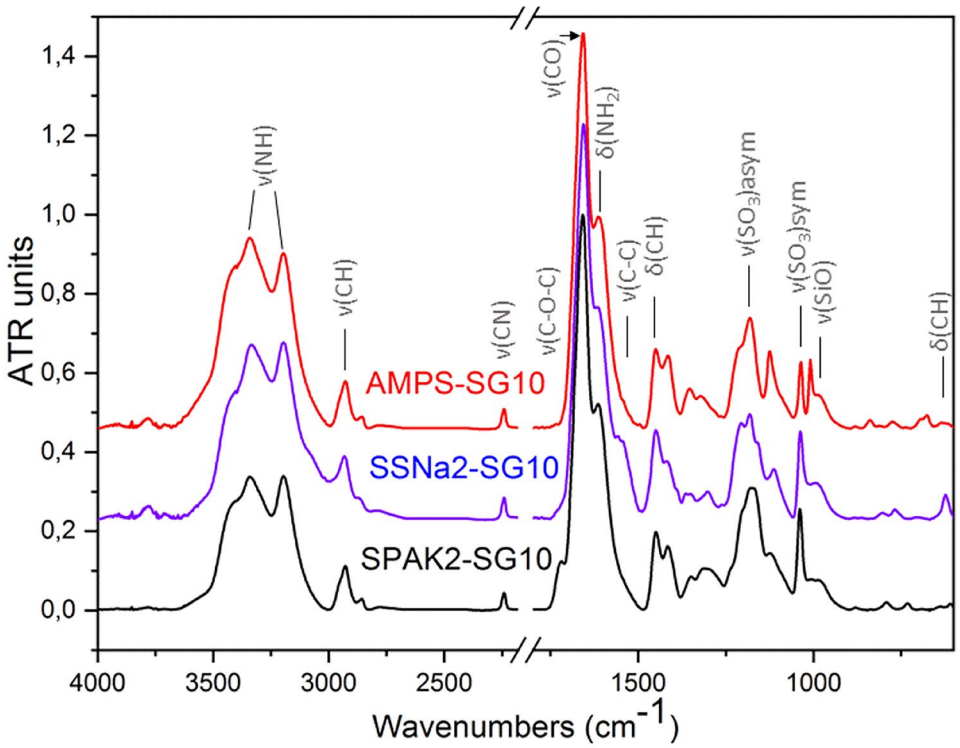

Fig. 2 FTIR spectra for composite hydrogels with various sulfo-containing components in polymer matrix

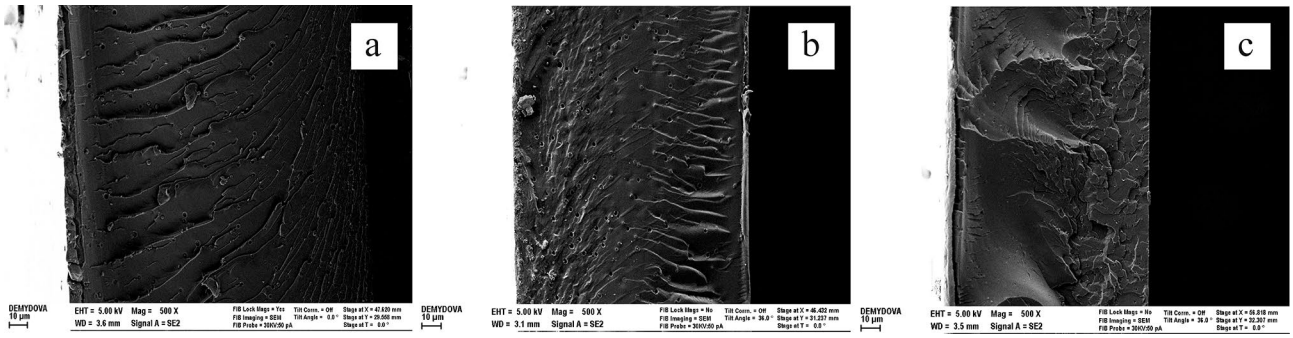

Fig. 3 SEM images of the cross-section for the polymer hydrogels: **a** SPAK-PH; **b** AMPS-PH; **c** SSNa-PH

morphology in the cross section. The top and middle layers are uniform, albeit with different morphologies, while the bottom layer shows greater heterogeneity. This can be explained by the fact that the hydrophilic component tends to "repel" the hydrophobic component toward the upper and lower surfaces of the sample and thereby causes the formation of a three-layer structure. As the hydrophilic network becomes less mobile with the propagation of polymerization, its main mass is accumulated in the middle layer. The incompatibility between the hydrophilic and hydrophobic components leads to microphase separation in the lower layer. The two-layer laminar structure of the SSNa containing membrane is also formed due to the redistribution of the hydrophilic/hydrophobic balance during the polymerization of the monomer mixture.

Figure 4 shows that the introduction of an inorganic component into the polymer matrix significantly affects the morphology of the hydrogel membranes. It is known from previous studies [28] that the addition of the sol–gel system various content to the SPAK-PH polymer composition leads to an improvement of the interphase interaction and promotes more homogeneous phase morphology. Such a compatibilizing effect also appears in hydrogels with AMPS and SSNa, probably due to a change in the hydrophilic/hydrophobic balance.

The results of the thermal stability study of the composite hydrogels are shown in Table 1. Three main areas of weight loss are observed in curve (Fig. 3) obtained by TGA. The first weight loss step is obviously related to the bounded water desorption for hydrophilic polymers. Therefore, two peaks in differential TGA thermogram of the AMPS-containing composite hydrogel (Fig. 5) assigned to trapped (first peak around 110 °C) and absorbed (second peak around 220 °C) water observed. In the temperature range from 180 °C to 350 °C, the second weight loss step is observed, as the initial processes of destruction of the polymer matrix take place: the degradation of lateral functional groups and cross-linking bonds. Such processes of thermal degradation lead to the final weight loss step in the temperature range of 350–550 °C. At this stage, the destruction of the polymer backbone occurs. In general, the thermal degradation behaviors of AMPS-PH, NaSS-PH, and SPAK-P membranes are similar with approximately the same mass loss. According to obtained results, all of these hydrogels respectively thermostable and could be used in the devices with operating temperature up to 250 °C.

The obtained DSC curves (Fig. 5) do not show exothermic (crystallization) or endothermic (melting) effects, but the glass transition process is observed. This effect is inherent in amorphous polymers and is associated with: a change in local degrees of freedom due to changes in twist angles

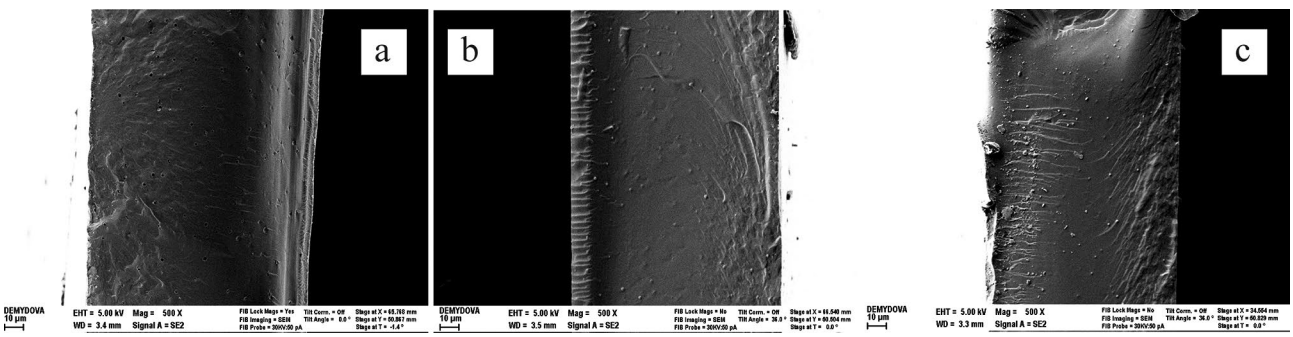

Fig. 4 SEM images for the composite hydrogel cross-sections: **a** SPAK-PH-SG10; **b** AMPS-PH-SG10; **c** SSNa-PH-SG10

Table 1 Thermal behavior of composite hydrogels with different sulfonate components

Sample name	I stage		II stage		III stage	
	T_{max}, °C	Weight loss, %	T_{max}, °C	Weight loss, %	T_{max}, °C	Weight loss, %
SPAK-PH-SG10	129	7.81	287	21.65	420	65.29
AMPS-PH-SG10	134	6.97	272	22.19	398	63.92
SSNa-PH-SG10	132	6.87	270	19.94	388	61.04

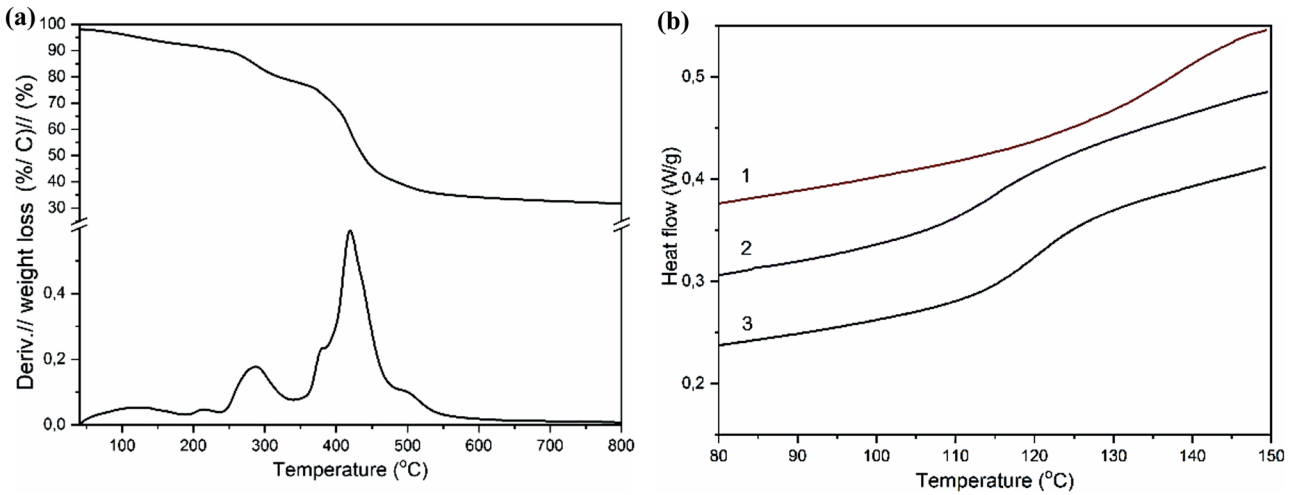

Fig. 5 **a** The integral and differential TGA thermograms for AMPS-PH-SG10; **b** DSC curves (II heating cycle) for composite hydrogels: 1—AMPS-PH-SG10; 2—SSNa-PH-SG10; 3—SPAK-PH-SG10

along the polymer matrix; the occurrence of segmental movements with the possibility of interaction with neighboring chains. The characteristics of the glass transition process for the polymers are given in Table 2. The synthesized materials have relatively high values of the glass-transition temperature. It should be noted that for organic/inorganic hydrogels, SPAK-PH-SG10 and SSNa-PH-SG10 T_g values practically do not differ; however, the glass transition temperature of AMPS-PH-SG10 hydrogels is somewhat higher.

It was suggested that the difference in water uptake values would have been triggered when sulfo-monomer type used in the synthesis of the polymer hydrogels change. The copolymer, which includes SSNa, has lower water uptake compared to copolymer, which includes AMPS and SPAK, apparently due to the fact that sulfo-groups of styrene sulfonate, directly attached to the benzene ring, reduce mobility of the molecules segments and increase hydrophobicity. The water uptake values of the sulfo-group-containing hydrogels with different composition after for 24 h in distilled water at 20 °C temperature are SPAK—1068 (±35)%, AMPS—945 (±39)%, SSNa—856 (±26)%, respectively. The obtained values of water uptake correspond about possibility to use these materials as a superabsordends.

Proton conductivity of the hydrogels is the most important characteristic for their use as conductive materials. The values of proton conductivity at room temperature (20 °C) of the synthesized hydrogels were obtained from the results of impedance spectroscopy, which are presented in the form of Nyquist diagrams in Fig. 6. As can be seen, the Nyquist plots are sloping straight lines, indicating good contact between the electrode and electrolyte. This behavior of the impedance histogram can be obtained due to the soft physical characteristics of the electrolyte films, and the same behavior was observed for all samples [28, 29]. The experimental data, presented as points on Nyquist plots, were modeled in the ZView2 software environment according to the equivalent circuit shown in the inset to Fig. 6. The equivalent circuit is a series connection of the volumetric resistance of the lectrolite R and the constant phase element CPE. The capacitive response of the measuring system is due to the use of blocking electrodes (platinum in our case). In this case, there is no discharge of ions and other reactions at the interface between

Table 2 Thermophysical properties of composite hydrogels with various sulfo-monomers

Parameters	AMPS-PH-SG10	SPAK-PH-SG10	SSNa-PH-SG10
T_{g2}, °C	133	116	113
ΔC_{p2}, Дж/г·К	0.65	0.63	0.59
$T_{g2} \cdot \Delta C_{p2}$, Дж/г	264	245	216

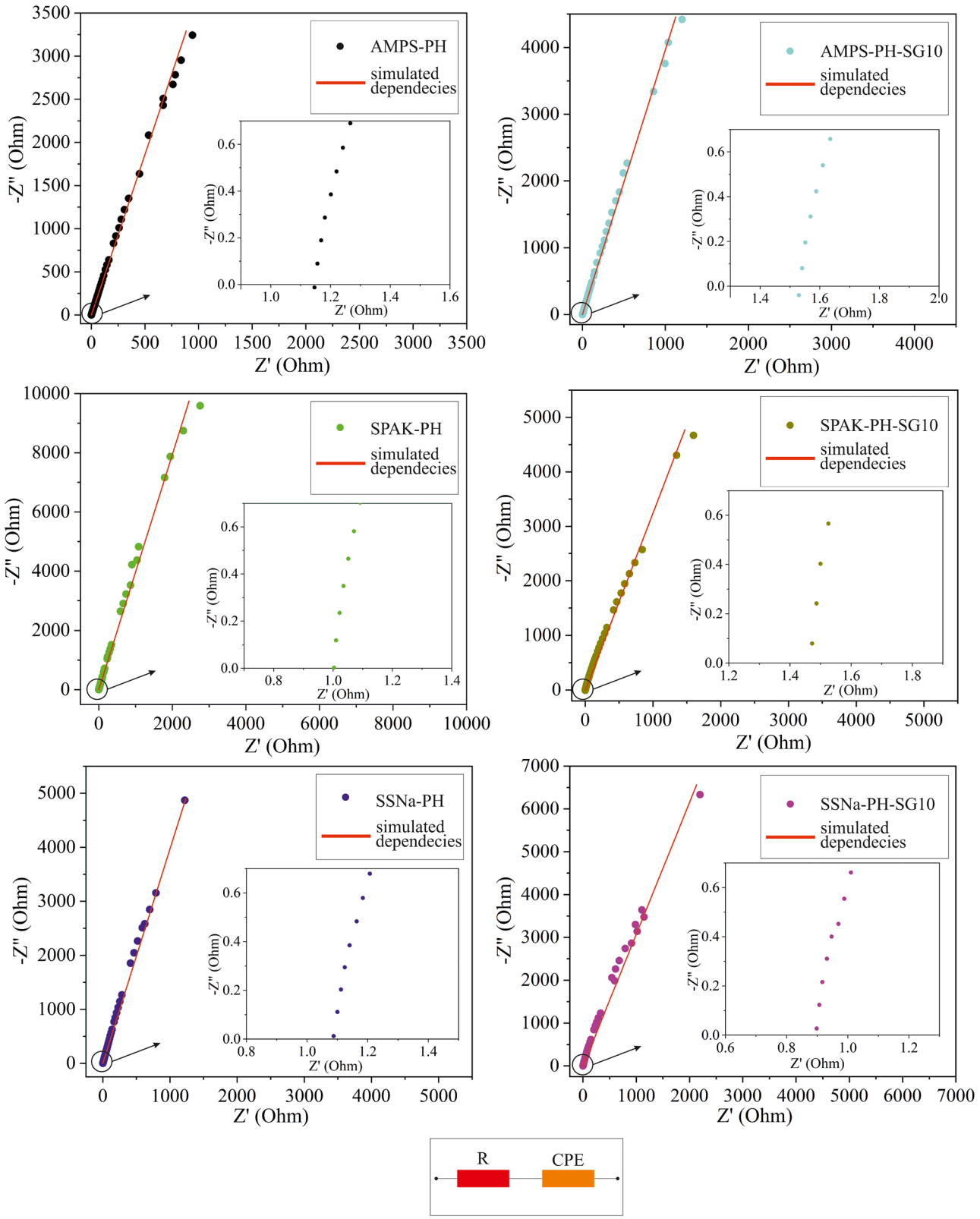

Fig. 6 Nyquist diagram for AMPS-PH, AMPS-PH-SG10, SPAK-PH, SPAK-PH-SG10, SSNa-PH, and SSNa-PH-SG10. The insets show the high-frequency part with high accuracy. The equivalent circuits for the studied heterostructures are also shown

the electrode and electrolyte, so the corresponding interface can be represented as the capacitance of a double electric layer. The typical value of such a capacitance is 10^{-6} F/cm^2. The CPE element used in the modeling is a generalized and universal tool for modeling the impedance of a wide class of electrochemical and other systems [30]. In our case, since the studied membranes are flat films, when studied in a wide frequency range, the wines will exhibit conductivity properties in a spatially limited region. It is also necessary to take into account the existence of air between the electrode and the membrane, which in practice will also be modeled by the CPE element.

The simplest description of the impedance of a constant-phase element can be given as.

$$Z_{CPE} = \frac{1}{A(j\omega)^n} \quad (2)$$

where A is the proportionality factor, $n = 0, 1, -1$ is the exponential factor, which denotes the phase deviation. For integer values of n, the CPE element degenerates to the classical elements with concentrated parameters R, C, and L, respectively. When modeling the experimental values (Fig. 6), the parameter n = 0.84 was used for all membranes. CPE (region C) gives the impedance of a pure or distributed element under the condition $n = 1\text{-}\varepsilon$, where e $0 \le \varepsilon < (0.1\text{–}0.2)$, which is fulfilled in our case. Accordingly, the capacitances C for all studied membranes determined by the modeling results are presented in Table 3. The modeling error did not exceed 5%.

The values of proton conductivity calculated by formula (1) for all the studied membranes are given in Table 3. The resistance values R were taken from experimentally measured data (see insets in Fig. 6). The area of the studied samples was the same, but they differed in thickness, so the l/S ratio for the membranes was different. The corresponding values are also shown in Table 3. The salt form of the SPAK and NaSS sulfo-groups had been transformed to acid form by immersion in 0.1 N hydrochloric acid solution for 24 h. The values of proton conductivity are relatively high, reaching 18.63 ± 0.62 mSm/cm for the composite hydrogel with AMPS motives in the polymer backbone. The high conductivities are attributed to fast proton transfer promoted by coexistence of large amounts of acidic -SO_3H groups and water molecules.

The values of proton conductivity increase in the row SSNa > SPAK > AMPS, which is correlated with the water uptake results. Generally, the hybrid hydrogels have the values of proton conductivity by 5–13% higher as compared to the polymer hydrogels. It evidences that the inorganic component sufficiently increases water uptake of the material.

Table 3 Values of the determined capacitive and conductive parameters for all studied hydrogels

Sample name	C, μF/cm^2	l/S, cm^{-1}	σ, mSm/cm	$\Delta\sigma$, mSm/cm
AMPS-PH	9.32	0.0205	17.70	0.59
AMPS-PH-SG10	6.63	0.0287	18.63	0.62
SPAK-PH	3.03	0.0141	14.01	0.46
SPAK-PH-SG10	7.00	0.0232	15.72	0.42
SSNa-PH	6.03	0.0145	13.29	0.44
SSNa-PH-SG10	5.28	0.0136	15.27	0.51

Conclusions

Cross-linked proton-conductive copolymer and composite hydrogels have been prepared using UV polymerization of the acrylate monomers. Sulfo-group-containing monomer content effects the morphology of the obtained hydrogels: copolymer membrane–containing SPAK has more homogeneous structure than the membranes with SSNa and AMPS, which possess an asymmetric laminar two- and three-layer structure, respectively. According to the TGA measurement, investigated composite hydrogels thermostable up to 250 °C. The higher value of proton conductivity riches up to 19 mSm/cm for composite AMPS-containing hydrogel, nonetheless for SSNa- and SPAK-containing hydrogels possess lower values. The suggested UV-derived hydrogels have good potential to be used as proton-conducting materials, superabsorbent. This method is user-friendly and cost-efficient, and proceeds in an aqueous environment under atmospheric conditions without the use of heavy metal catalysts.

Acknowledgements Khrystyna Rymsha gratefully acknowledges German Academic Exchange Service (DAAD) for financial support (Research Grants for Doctoral Candidates and Young Academics and Scientists 2015/16, program ID 57130104). Authors also thank Dr. Mikhail Malanin for his help with FTIR measurements, Dr. Liane Häußler for her TGA and DSC measurements, and Dr. Andriy Horechyy for the helpful discussion.

References

1. Peng Q, Chen J, Wang T, Peng X, Liu J, Wang X, Wang J, Zeng H et al (2020) Recent advances in designing conductive hydrogels for flexible electronics. InfoMat 2(5):843–865. https://doi.org/10.1002/inf2.12113
2. Wang W, Narain R, Zeng H et al (2018) Rational design of self-healing tough hydrogels: a mini review. Front Chem 6:497. https://doi.org/10.3389/fchem.2018.00497
3. Sun JY, Zhao X, Illeperuma WRK, Chaudhuri O, Oh KH, Mooney DJ, Vlassak JJ, Suo Z et al (2012) Highly stretchable and tough hydrogels. Nature 489:133–136. https://doi.org/10.1038/nature11409
4. Tavakoli J, Tang Y (2017) Hydrogel based sensors for biomedical applications: an updated review. Polymers 9:364. https://doi.org/10.3390/polym9080364
5. Huang S, Liu Y, Zhao Y, Ren Z, Guo CF et al (2019) Flexible electronics: stretchable electrodes and their future. Adv Funct Mater 29:1805924. https://doi.org/10.1002/adfm.201805924
6. Sampath S, Choudhury N, Shukla A et al (2009) Hydrogel membrane electrolyte for electrochemical capacitors. J Chem Sci 121(5):727–734. https://doi.org/10.1007/s12039-009-0087-7
7. Walker BW, Portillo Lara R, Mogadam E, Hsiang YC, Kimball W, Annabi N et al (2019) Rational design of microfabricated electroconductive hydrogels for biomedical applications. Prog Polym Sci 92:135–157. https://doi.org/10.1016/j.progpolymsci.2019.02.007
8. Chandra S, Sekhon S, Srivastava R, Arora N et al (2002) Proton-conducting gel electrolyte. Solid State Ion 154–155(2):609–619. https://doi.org/10.1016/S0167-2738(02)00505-2
9. Zhao F, Bae J, Zhou X, Guo Y, Yu G et al (2018) Nanostructured functional hydrogels as an emerging platform for advanced energy technologie. Adv Mater 30:1801796. https://doi.org/10.1002/adma.201801796
10. Bao Z, Chen X (2016) Flexible and stretchable devices. Adv Mater 28:4177–4179. https://doi.org/10.1002/adma.201601422
11. Lee HR, Kim CC, Sun JY et al (2018) Stretchable ionics – a promising candidate for upcoming wearable devices. Adv Mater 30:1704403. https://doi.org/10.1002/adma.201704403
12. Li L, Lou Z, Chen D, Jiang K, Han W, Shen G et al (2018) Recent advances in flexible/stretchable supercapacitors for wearable electronics. Small 14:1702829. https://doi.org/10.1002/smll.201702829
13. Rong Q, Lei W, Liu M et al (2018) Conductive hydrogels as smart materials for flexible electronic devices. Chem A Eur J 24:16930–16943. https://doi.org/10.1002/chem.201801302
14. Choudhury NA, Prashant SK, Pitchumani S, Sridhar P, Shukla AK et al (2009) Pol (vinyl alcohol) hydrogel membrane as electrolyte for direct borohydride fuel cells. J Chem Sci 121(5):647–654. https://doi.org/10.1007/s12039-009-0078-8
15. Chen B, Bai Y, Xiang F, Sun J-Y, Chen YM, Wang H, Zhou J, Suo Z et al (2014) Stretchable and transparent hydrogels as soft conductors for dielectric elastomer actuators. J Polym Sci B 52:1055–1060. https://doi.org/10.1002/polb.23529
16. Liu J, Tan CSY, Yu Z, Li N, Abell C, Scherman OA et al (2017) Tough supramolecular polymer networks with extreme stretchability and fast room-temperature self-healing. Adv Mater 29:1605325. https://doi.org/10.1002/adma.201605325
17. Biondi M, Borzacchiello A, Mayol L, Ambrosio L et al (2015) Nanoparticle-integrated hydrogels as multifunctional composite materials for biomedical applications. Gels 1:162–178. https://doi.org/10.3390/gels1020162
18. Annabi N, Tamayol A, Uquillas JA, Akbari M, Bertassoni LE, Cha C, Camci-Unal G, Dokmeci MR, Peppas NA, Khademhosseini A et al (2014) 25th anniversary article: rational design and applications of hydrogels in regenerative medicine. Adv Mater 26:85–123. https://doi.org/10.1002/adma.201303233
19. Choi S, Lee H, Ghaffari R, Hyeon T, Kim DH et al (2016) Recent advances in flexible and stretchable bio-electronic devices integrated with nanomaterials. Adv Mater 28:4203–4218. https://doi.org/10.1002/adma.201504150
20. Copello GJ, Mebert AM, Raineri M, Pesenti MP, Diaz LE et al (2011) Removal of dyes from water using chitosan hydrogel/SiO2 and chitin hydrogel/SiO2 hybrid materials obtained by the sol–gel method. J Hazard Mater 186:932–939. https://doi.org/10.1016/j.jhazmat.2010.11.097
21. Demydova K, Horechyy A, Meier-Haack J, Malanin M, Häußler L, Stamm M, Yevchuk I, Demchyna O et al (2020) Hybrid organic-inorganic materials on the basis of acrylic monomers and TEOS prepared by simultaneous UV-curing and sol-gel process. J Polym Res 27:88. https://doi.org/10.1007/s10965-020-02057-w
22. Grigoraviciute-Puroniene I, Yevchuk I, Demchyna O, Zhyhailo M, Rymsha K, Babkina N et al (2022) Proton-conducting organic-inorganic sulfo-containing membranes for fuel cell. Mater Sci 28(1):82–88. https://doi.org/10.5755/j02.ms.28440
23. Zhyhailo M, Yevchuk I, Yatsyshyn M, Korniy S, Demchyna O, Musiy R, Raudonis R, Zarkov A, Kareiva A et al (2020) Preparation of polyacrylate/silica membranes for fuel cell application by in situ UV polymerization. Chemija 31(4):247–254. https://doi.org/10.6001/chemija.v31i4.4321
24. Pal S, Mondal R, Guha S, Chatterjee U, Jewrajka SK et al (2019) Homogeneous phase crosslinked poly(acrylonitrile-co-2-acrylamido-2-methyl-1-propanesulfonic acid) conetwork exchange membranes showing high electrochemical properties and electrodialysis performance. Polymer 180:121680. https://doi.org/10.1016/j.polymer.2019.121680
25. Zhyhailo M, Horechyy A, Meier-Haack J, Formanek P, Malanin M, Arnhold K, Schneider K, Yevchuk I, Fery A et al (2021) Proton conductive membranes from covalently cross-linked poly(acrylate)/silica interpenetrating networks. Macromol Mater Eng 306(4):2000776. https://doi.org/10.1002/mame.202000776
26. Ding X, Jia R, Gan Z, Du Y, Wang D, Xu X et al (2020) Tough and conductive polymer hydrogel based on double network for photo-curing 3D printing. Mater Res Express 7:055304. https://doi.org/10.1088/2053-1591/ab8cfb
27. Maeda S, Fujiwara Y, Sasaki C, Kunimoto K-K et al (2012) Structural analysis of microbial poly(ε-L-lysine)/poly(acrylic acid) complex by FT-IR, DSC, AHd solid-state 13C and 15N NMR. Polym J 44:200–203. https://doi.org/10.1038/pj.2011.108
28. Ali AMM, Subban RHY, Bahron H, Winie T, Latif F, Yahya MZA et al (2008) Grafted natural rubber-based polymer electrolytes: ATR-FTIR and conductivity studies. Ionics 14:491–500. https://doi.org/10.1007/s11581-007-0199-3
29. Vyas MK, Chandra A (2016) Ion–electron-conducting polymer composites: promising electromagnetic interference shielding material. ACS Appl Mater Inter 8:18450–18461. https://doi.org/10.1021/acsami.6b05313
30. Barsoukov E, Macdonald JR, editors Impedance spectroscopy: theory, experiment, and applications. John Wiley & Sons, Inc., Hoboken, New Jersey Canada. 205-595